Supplementary Information

Laser-patterned epoxy-based 3D microelectrode arrays for extracellular recording

Hu Peng [a], Inola Kopic [a], Shivani Ratnakar Potfode [a], Tetsuhiko Teshima [a,b*], George Al Boustani [a], Lukas Hiendlmeier [a], Chen Wang [d], Mian Zahid Hussain [c], Berna Özkale Edelmann [d], Roland A. Fischer [c], and Bernhard Wolfrum [a,b*]

[a] *Neuroelectronics, Munich Institute of Biomedical Engineering, Department of Electrical Engineering, TUM School of Computation, Information and Technology, Technical University of Munich, Hans-Piloty-Str. 1, 85748, Garching, Germany*

[b] *Medical & Health Informatics Laboratories NTT Research Incorporated 940 Stewart Dr, Sunnyvale, CA 94085, USA*

[c] *Chair of Inorganic and Metal-Organic Chemistry, School of Natural Sciences and Catalysis Research Center, Department of Chemistry, Technical University of Munich, Lichtenbergstr. 4, 85748 Garching, Germany*

[d] *Microrobotic Bioengineering Lab (MRBL), Department of Electrical Engineering, TUM School of Computation, Information, and Technology, Technical University of Munich, Hans-Piloty-Str 1, Garching 85748, Germany*

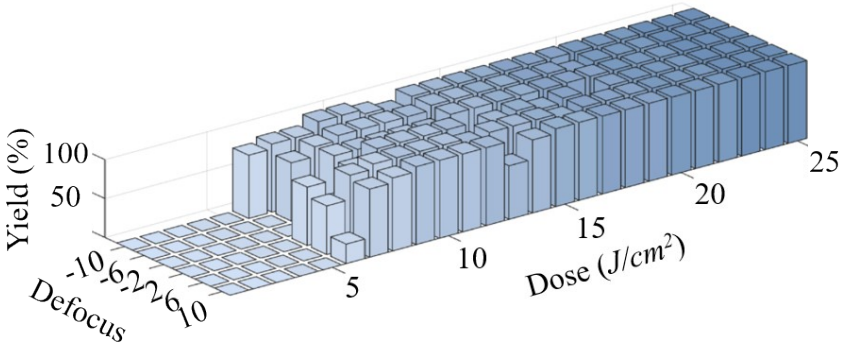

Fig. S1 Parameterization of the photolithography process.

To obtain reproducible pillars, we parameterized the defocus parameter ranging from -10% to +10% of the working distance and the dose ranging from 0 to 25 J/cm^2. Fig. S1 shows the yield for epoxy-based pillar formation after development in dependence on dose and defocus parameters. When the dose reaches 18 J/cm^2 with a defocus of + 10, nearly 100% of epoxy-based pillars were well-developed. The same parameters were chosen for the fabrication of pillars, as shown in Fig. 3. A shorter exposure time can be reached by selecting the minimal dose with sufficient yield or increasing the power of the light source.

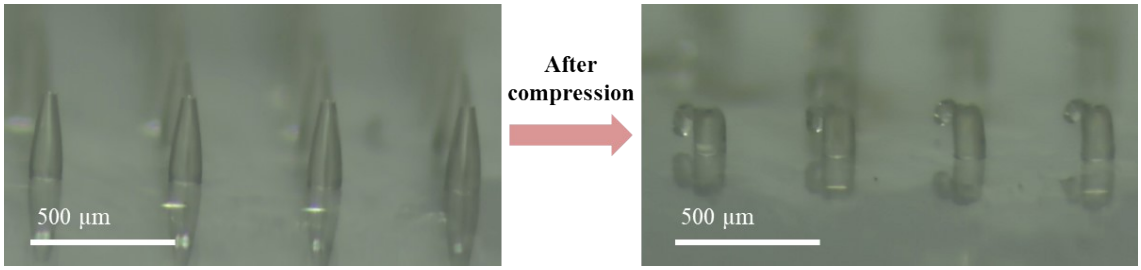

Fig. S2 Optical image of deformed pillars after compressive force measurement.

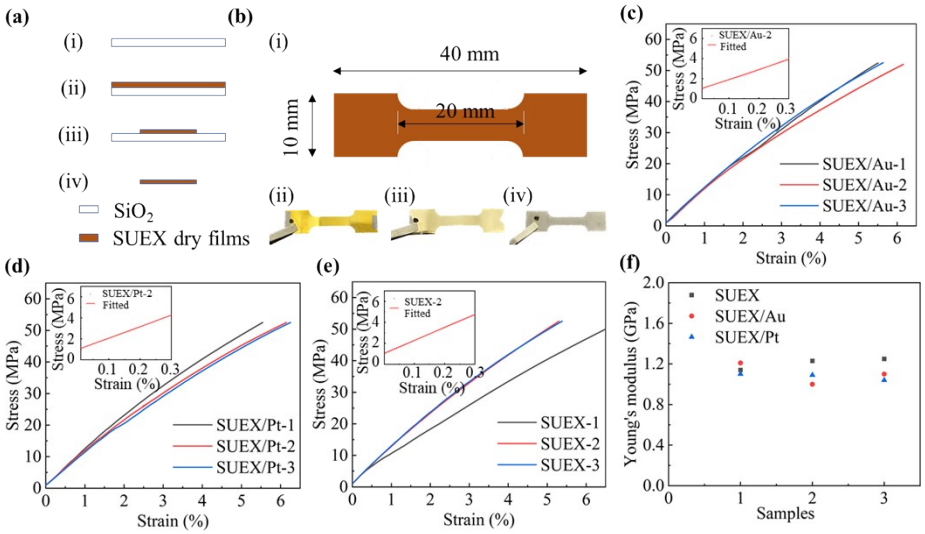

Fig. S3 Young's modulus measurements of epoxy-based structures. (a-b) A schematic of the fabrication and measurements. Strain vs. stress curves of (c) SUEX covered by a layer of 100 nm Au, (d) SUEX covered by a layer of 100 nm Pt, and (e) bare SUEX dry films. (f) calculated Young's modulus of SUEX/Au, SUEX/Pt, and bare SUEX. The inset figures in (c) to (e) are the linear fitting curves from 0 to 0.3%.

To calculate the Young's modulus difference of bare SUEX dry film, SUEX/Pt, and SUEX/Au, a structure shown in Fig. S2(b, ⅰ) was prepared. Firstly, glass substrates were cleaned with acetone, isopropanol, and deionized water successively (Fig. S2(a, ⅰ). Afterward, SUEX films with a thickness of 200 µm were laminated onto the clean glass substrate (Fig. S2(a, ⅱ)). An optical lithography process was applied to pattern the desired structure, as seen in Fig. S2(a, ⅲ). In the last step, the structure was peeled off from the glass substrate. Afterward, 10 nm Ti/100 nm Au (Fig. S2(b, ⅱ)) or 10 nm Ti/100 nm Pt (Fig. S2(b, ⅲ)) were sputtered onto the structures' surface, Fig S2(b, ⅳ) represents the bare SUEX sample.

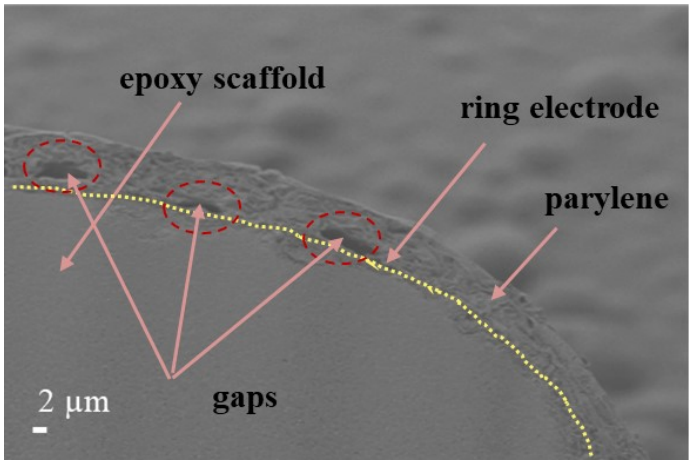

Fig. S4 A close-up SEM image of an individual ring electrode at the tip of the pillar; the dotted yellow line indicates the electrode area. Gaps at the interface indicate an additional exposed electrode area.

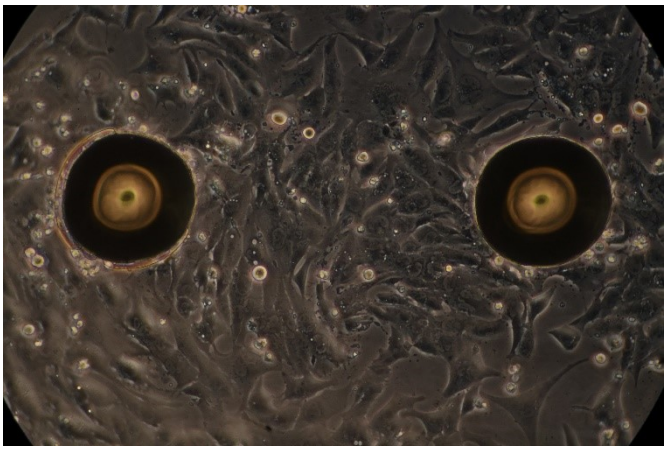

Fig. S5 Optical image of cells growing on a chip.

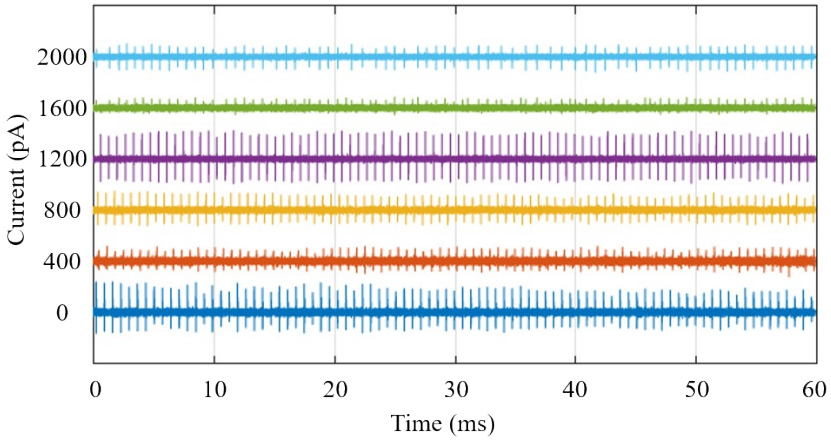

Fig. S6 Spontaneous action potentials recorded from 6 channels. It shows the spontaneous action potentials recorded from 6 channels for 60 seconds. A current offset of 400 pA is shown on the y-axis to visualize the individual channels more clearly.

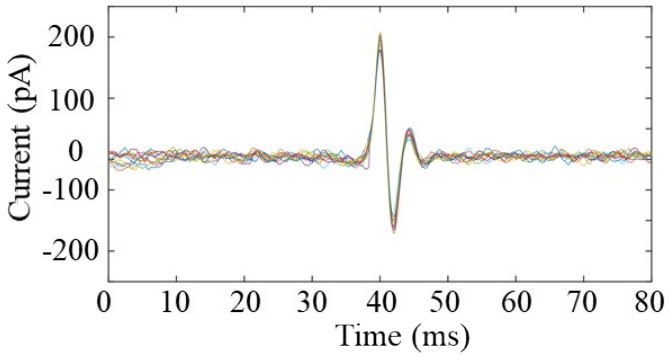

Fig. S7 Superposition of 12 spikes, recorded with the same 3D electrode.